Supplementary Sections and Tables

Supplementary Section S1: Causal Parameters and Experimental Readouts for CAF-Driven Transport Phenotyping

When the extracellular matrix is treated as the primary causal input in the stromal–transport framework, a range of structural, mechanical, and molecular parameters can be quantified to characterize CAF-driven remodeling and its transport consequences.

Structural and mechanical input parameters include:

(A) ECM stiffness, measured by atomic force microscopy (AFM), bulk rheology or second-harmonic generation (SHG) imaging, providing a readout of collagen density, crosslinking, and matrix tension.[1,2]

(B) ECM chemical composition, including collagen and hyaluronan content, the expression of distinct collagen types (e.g., COL1A1, COL3A1), and crosslinking enzymes (e.g., LOX family), quantified by immunoassays, transcriptomics, proteomics, or high-performance liquid chromatography.[3–8]

(C) Matrix porosity, assessed by tracer exclusion assays or imaging modalities such as diffusion-sensitive optical coherence tomography or AFM-based mapping.[9–11]

(D) Intrinsic permeability, measured by pressure-drop assays, plastic compression combined with Darcy's law analysis, or tracer flow tracking through ECM-filled channels.[12–15]

Cellular and mechanotransduction output parameters include:

(E) Transcriptomic and chromatin accessibility profiles, obtained by single-cell RNA sequencing (scRNA-seq) and ATAC-seq, enabling identification of CAF states and mechanotransduction programs.[16]

(F) Mechanosensitive signaling markers, such as nuclear localization of YAP/TAZ or activation of related pathways, which report cellular responses to matrix stiffness and stress.[17–20]

(G) Functional cellular readouts, including contractility, proliferation, and migratory behavior of CAFs and cancer cells.[5,21]

Together, these parameters define the experimental space in which causal relationships between CAF-driven ECM remodeling and transport phenotypes can be tested, either by perturbing stromal inputs and measuring transport outputs or by directly modifying matrix properties and observing cellular responses.

Supplementary Table S1 Symbols, units, and measurement readouts

Quantity (symbol)	Meaning	Units	Primary on-chip readouts / assays	Notes
c	Solute concentration (drug, tracer)	$mol \cdot m^{-3}$ (or a.u. via fluorescence)	Fluorescence intensity maps sampled effluent concentration[22,23]	Convert a.u. to concentration via calibration curve when possible.
D_{eff}	Effective diffusivity in ECM / tissue	$m^2 \cdot s^{-1}$	FRAP/photobleaching; time-lapse penetration profiles; FCS[24]	Depends on porosity, tortuosity, solute size; report tracer MW and charge.
D_0	Free diffusivity in solvent (no matrix)	$m^2 \cdot s^{-1}$	Literature values; measured in blank gel-free channel[25,26]	Use same temperature/viscosity conditions as experiments.

ϕ	Porosity / void fraction (fluid volume fraction)	dimensionless	Swelling/solid content; imaging-based pore/mesh inference; permeability–porosity fits[27]	Often inferred rather than directly measured; state method clearly.
λ	Tortuosity factor	dimensionless	Estimated from D_0/D_{eff} relationship (λ = sqrt(D_0/D_{eff}) when applicable)[28]	An effective descriptor It does not uniquely capture pore connectivity.
q	Darcy volumetric flux	$m \cdot s^{-1}$	From imposed flow rate and cross-sectional area; particle image velocimetry (PIV)[29–31]	Use when flow through porous gel is controlled/known.
k	intrinsic permeability (intrinsic)	m^2 (intrinsic)	Pressure-driven flow through gel; pressure-decay/relaxation assays; poroelastic fits[30]	Sensitive to gel compaction and boundary leakage; report gel confinement/anchoring.
p, Δp	Interstitial fluid pressure and pressure gradient	Pa (or mmHg)	On-chip pressure sensors; manometry; hydrostatic head differences[32]	State boundary conditions; high IFP reduces convective delivery.
v_p	Interstitial (pore) velocity	$m \cdot s^{-1}$	Tracer front tracking; PIV; derived from q/φ[33]	Local vp can be heterogeneous; report mean and spatial maps if possible.
E	Elastic modulus (matrix/tissue)	Pa (often kPa)	Indentation; AFM; microbead rheology; elastography[34,35]	Report strain rate and method; ECM remodeling changes E over time.
η	Viscous modulus/relaxation parameter	Pa·s	Stress relaxation/creep assays; poroviscoelastic fits[36]	Useful for time-dependent deformation and transport coupling.
σ, ε, u	Stress, strain, displacement field	Pa; dimensionless; m	Traction force microscopy; displacement tracking; applied compression gauges[37]	Often captured as global applied stress/strain in ToC; local mapping is advanced.
α, M	Biot coefficient; Biot (storage) modulus	dimensionless; Pa	Estimated by fitting poroelastic pressure-relaxation data[38]	Include only if using coupled poroelastic models; can be lumped in simplified fits.
R	Reaction term (uptake/clearance/production)	$mol \cdot m^{-3} \cdot s^{-1}$	Cellular uptake kinetics from time-course depletion; imaging of internalization markers[39]	Separate cellular uptake from binding/sorption when possible.
c_s, K_d	Adsorbed/immobile solute; partition coefficient	$mol \cdot m^{-3}$; $m3 \cdot mol^{-1}$ (or dimensionless)	Device/gel adsorption tests (% recovery); mass balance in controls[40,41]	Critical for PDMS and hydrophobic drugs; include controls.

Supplementary Section S2: Experimental and Computational Calibration of Transport Parameters

A wide array of tumor-transport frameworks has been developed over the past decade, ranging from continuous advection–diffusion–reaction models to multi-physics simulations incorporating vascular flow, interstitial

pressure, and matrix mechanics.[22,42–44] Among these, the coupled advection–diffusion–Darcy–poroelastic (or poroviscoelastic) framework strikes a practical balance between mechanistic richness and mathematical tractability.[45–49] It captures the essential couplings among diffusion, advection, reaction, and solid mechanics, while remaining amenable to numerical solution and parameter estimation.[48,50]

In practice, model calibration often begins by treating parameters such as effective diffusivity D_{eff}, intrinsic permeability k, and reaction rates R as spatially averaged constants fitted to bulk tracer uptake or release data.[28,51]

Fluorescent tracer penetration in hydrogels or tissue slices is quantified by microscopy or FRAP, and the resulting concentration profiles are simulated with transport equations to infer D_{eff}.[52,53] Such indirect estimation is often necessary because diffusivity cannot be measured directly in heterogeneous biological materials.[54]

More advanced strategies aim to resolve spatial and temporal heterogeneity. Tracer diffusion measurements (FRAP, FCS) can be combined with pressure-relaxation or compression assays to constrain both transport and mechanical parameters.[10,55] Pressure-relaxation experiments analyzed using Darcy–Biot poroelastic models provide direct estimates of intrinsic permeability k and elastic modulus E, including their strain dependence.[47,49,56] These parameters can be combined into effective transport coefficients (e.g., $D \sim kM/\mu$) used in advection–diffusion simulations.[57,58]

Controlled hydrogel systems are particularly useful for calibration because crosslinking density, porosity, and polymer content can be varied independently.[24,59] Studies using GelMA and PEGDA hydrogels demonstrate that modest changes in crosslinking or mesh size can lead to orders-of-magnitude differences in diffusivity and permeability.[24,59,60] For example, 5% bovine serum albumin (66.5 kDa) formulation diffuses more than an order of magnitude faster in GelMA than when at 10%.[61] Intrinsic permeability similarly varies by several orders of magnitude between weakly and highly crosslinked gels. Comparable trends are observed in PEGDA systems, with stronger restrictions for large macromolecules than for small solutes such as glucose.[24,59,60,62–64]

These empirical relationships provide functional links between matrix density, porosity, and transport parameters that can be incorporated into models, e.g. $D_{eff} = F[\phi]$.[54] However, structural descriptors such as porosity alone are insufficient: matrices with identical porosity can differ by an order of magnitude in permeability due to differences in pore connectivity and topology.[65,66]

Biological variability introduces an additional layer of complexity.[67,68] Primary fibroblasts from different donors can display large differences in ECM production, thickness, and mechanical strength even under standardized conditions. For example, dermal fibroblasts from different individuals showed up to 3.2-fold variation in ECM perforation strength and 2.5-fold variation in collagen content.[69] Such variability can be exploited experimentally by constructing matrices with defined CAF compositions and measuring how tracer penetration or drug response changes accordingly.[70]

Temporal evolution further complicates calibration.[71–73] Models that fit early time points (e.g., day 3) may fail at later times (day 7 or beyond) because cells polarize, differentiate, and remodel the matrix.[74,75] Hydrogel contraction, phenotypic drift, and ECM maturation progressively alter transport properties, creating an intrinsic mismatch between short-term in vitro assays and long-term *in vivo* disease progression.[76–79]

Finally, technical variability remains substantial. Inter-laboratory studies report 35% variation and up to six-fold differences in diffusion measurements using nominally identical materials and protocols.[80,81] Diffusion-based estimates of permeability can differ by an order of magnitude from flow-based measurements, especially at high collagen density, highlighting the sensitivity of transport assays to compression, handling, and flow history.[13,22]

Supplementary Section S3: Strategies to Modulate CAF-Driven Matrix Barriers and Transport Phenotypes

CAF-driven remodeling of the extracellular matrix generates dynamic transport barriers that restrict drug and immune-cell access in many solid tumors.[82–90] Because these barriers arise from identifiable biological and physical mechanisms, they can be transiently modulated. This section summarizes experimental strategies to alter CAF-mediated matrix structure, mechanics, and transport properties, providing a methodological toolbox that complements the transport-phenotyping framework developed in the main text.

Enzymatic modulation of the extracellular matrix: Proteolytic remodeling represents a direct approach to transiently increase matrix porosity and permeability. Matrix metalloproteinases (MMPs), A Disintegrin And Metalloproteinases (ADAMs), and exogenous collagenases can degrade fibrillar collagens and proteoglycans, thereby enlarging pore size and reducing tortuosity.[91–94] Such interventions have been shown to enhance penetration of small molecules, antibodies, and nanoparticles in dense collagen matrices.[94–96]

Matrix degradation is tightly regulated in vivo by Tissue Inhibitors of Metalloproteinases (TIMPs 1–4), which balance ECM turnover. Experimental modulation of TIMP levels, either by inhibition or overexpression, provides an additional lever to fine-tune proteolytic activity. However, nonselective ECM degradation can promote tumor invasion, angiogenesis, or inflammation, highlighting the need for controlled dosing, spatial targeting, and temporal sequencing.[91,93,97,98] To address these limitations, enzyme-loaded delivery systems, such as collagenase-functionalized nanoparticles ("collagozomes"), have been developed to localize matrix degradation and limit systemic exposure.[94,95] These strategies demonstrate that enzymatic remodeling can open transient transport windows, but their clinical translation requires careful evaluation of safety and context dependence.

Mechanical modulation of stromal barriers: Mechanical forces strongly influence ECM architecture and transport. Experimental compression of collagen networks reduces intrinsic permeability and diffusivity by increasing fiber density and decreasing pore connectivity.[13,99,100] Conversely, mechanical stress relief or decompression can restore fluid pathways and enhance solute transport.[101–103]

Microfluidic and tissue-engineered systems allow controlled application of compressive or tensile loads, enabling systematic investigation of strain-dependent transport. Pressure–relaxation and compression assays analyzed with poroelastic or poroviscoelastic models quantify how mechanical deformation alters permeability and elastic moduli.[48,79,104] Such approaches reproduce key features of desmoplastic tumors, including solid stress accumulation and vessel compression, and provide a platform to test mechanical normalization strategies.

Pharmacological reprogramming of CAF activity: Rather than directly degrading the matrix, stromal barriers can be modulated upstream by targeting CAF activation and function. Inhibition of TGF-β signaling, LOX-mediated crosslinking, or transglutaminase activity reduces matrix deposition and stiffness, thereby indirectly increasing porosity and permeability. [98,105–107] These interventions alter the coefficients governing transport (e.g., D_{eff}, k, and p) by reshaping CAF-driven remodeling programs. Because CAF populations are heterogeneous and context dependent, the effects of such interventions vary across tumor types and patients. Tumor-on-chip platforms enable systematic testing of CAF reprogramming strategies under controlled conditions, allowing transport phenotypes to be measured before and after perturbation and facilitating identification of responsive stromal states.[108–110]

Nanocarrier-based delivery strategies: Nanomedicine approaches aim to improve drug delivery by engineering carriers that navigate dense ECM environments. Carrier size, shape, surface charge, and stiffness critically influence penetration through CAF-remodeled matrices.[82,111,112] Larger nanoparticles are more strongly hindered by reduced pore size and tortuosity, whereas smaller or deformable carriers may achieve deeper penetration. Microfluidic models have been used extensively to quantify size-dependent transport and to evaluate how matrix remodeling alters nanocarrier distribution.[113–115] While nanocarriers offer potential advantages, their performance remains constrained by the same transport barriers that limit free drug diffusion, reinforcing the importance of understanding and modulating stromal transport properties.

Biomarkers linked to transport phenotypes: A key goal of transport phenotyping is to identify measurable biomarkers that reflect the strength of the stromal barrier. Candidate biomarkers include ECM stiffness, collagen density and organization, intrinsic permeability, interstitial pressure, and CAF composition.[1,116–118] Imaging modalities, histological analysis, and on-chip measurements can be combined to associate these features with transport coefficients extracted from modeling. Such biomarkers provide a bridge between experimental transport phenotyping and clinical stratification, enabling identification of tumors likely to benefit from stromal modulation or from specific therapeutic sequencing strategies.

Integration with transport phenotyping frameworks: Collectively, the strategies described above illustrate that CAF-driven transport barriers are dynamic and potentially reversible.[103,119,120] When combined with quantitative transport measurements and modeling, these interventions enable causal testing of how specific stromal mechanisms regulate drug accessibility. In this context, enzymatic, mechanical, pharmacological, and nanocarrier-based approaches are best viewed not as standalone therapies, but as tools to probe and manipulate transport phenotypes within a unified experimental–computational framework.

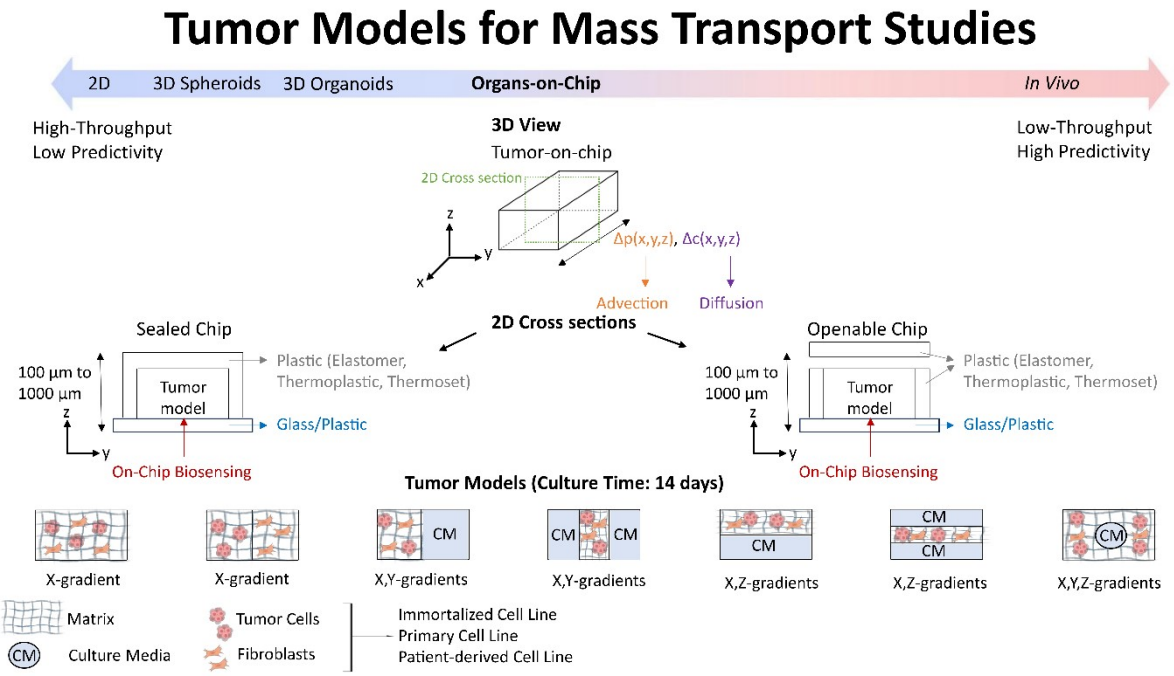

Supplementary Figure S1. Overview of tumor models used for mass transport studies. Comparative schematic illustrating five commonly used tumor model types, arranged from left to right in increasing order of biological complexity and physiological relevance: 2D monolayer, 3D spheroid, 3D organoid, tumor-on-chip, and in vivo tumors. For tumor-on-chip (ToC) systems, cross-sectional schematics highlight two frequently used configurations: sealed and openable chips, illustrating the spatial organization of tumor cells, fibroblasts, extracellular matrix, and surrounding culture medium. This overview emphasizes the trade-off between experimental controllability and in vivo relevance and provides contextual support for the positioning of ToC platforms in transport-focused studies.

Supplementary Table S2 Device structural materials and implications for transport assays

Material	Category	Key transport-relevant properties	Strengths	Limitations / risks
PDMS[121]	Elastomer	Gas-permeable; hydrophobic; high	Rapid prototyping; optical clarity; easy	Dose depletion for hydrophobic drugs; altered PK/PD; batch

		small-molecule sorption; can leach oligomers	bonding	variability
COC/COP[128]	Thermoplastic	Low sorption; good optical; rigid	Improved PK fidelity; scalable manufacturing	Fabrication/bonding complexity vs PDMS
PS[129]	Thermoplastic	Low-to-moderate sorption; cell-culture familiarity	Standard workflows; compatibility with plates	Less flexible microfabrication; solvent sensitivity
PMMA[130]	Thermoplastic	Rigid; optical; moderate sorption	Machinable; low-cost	Solvent swelling; bonding constraints
OSTE[131]	Polymer (thiol–ene)	Low sorption; tunable surface chemistry; robust bonding	Middle ground between PDMS and thermoplastics	Less standardized; fewer long-term benchmarks
Glass[132]	Inorganic	Minimal sorption; hydrophilic	Best for quantitative assays; stable	Microfabrication cost; integration complexity
Silicon[133]	Inorganic	Minimal sorption; precise microfabrication	High precision; stable	Opaque (often) and costly; niche
Parylene-C coating[134]	Surface coating	Reduces sorption; inert barrier	Improves PK fidelity in polymer devices	Adds process step; potential delamination if poorly applied
APTES / Silanization[135]	Surface functionalizatio n	Adds reactive groups for gel anchoring	Robust gel confinement	Requires careful process control
Polydopamine (PDA)[136]	Surface coating	Universal adhesive for protein-based gels	Works across substrates; simple	Batch/aging effects
3D-printed resins[137]	Additive materials	Variable chemistry; potential leachables; autofluorescence	Rapid prototyping of complex geometry	Standardization/biocompatibilit y concerns; sorption unknown

Supplementary Section S4: Device structural materials and transport artefacts

The choice of microfluidic device materials critically affects transport measurements, particularly for small molecules and hydrophobic drugs. Polydimethylsiloxane (PDMS) has long been used due to its optical transparency, gas permeability, and ease of fabrication via soft lithography. However, PDMS exhibits significant absorption of hydrophobic compounds and can leach uncured oligomers, progressively altering the effective delivered dose and confounding pharmacokinetic and pharmacodynamic readouts.[41,121,122]

To mitigate these effects, rigid thermoplastics such as cyclic olefin copolymer (COC), cyclic olefin polymer (COP), polystyrene (PS), and polymethyl methacrylate (PMMA) are increasingly adopted for transport-focused tumor-on-chip (ToC) systems. These materials maintain geometric stability under perfusion (outlined in supplemental Figure S3) and exhibit substantially reduced small-molecule partitioning compared to PDMS. Among them, COC and COP are particularly well-suited for quantitative transport studies due to their low drug sorption and chemical inertness.[123,124]

Surface chemistry further modulates transport artefacts and matrix integration. Covalent functionalization strategies such as silanization (e.g., APTES) introduce reactive groups that promote hydrogel anchoring, while polydopamine coatings provide a versatile adhesive interface compatible with protein-based matrices. Parylene-C coatings are frequently employed to suppress hydrophobic drug absorption while preserving optical clarity.

When appropriately combined, these strategies stabilize matrix confinement and improve the reproducibility of transport measurements.[125–127]

Supplementary Table S3 Hydrogels/ECM choices for CAF-driven transport phenotyping

Hydrogel / ECM	Why used	How to tune transport properties	Transport readouts enabled	Common pitfalls
Collagen I[22,154,155]	Native ligand-rich; proteolytically remodelable; standard for stromal models	Concentration; pH/temperature; crosslinking; confinement to induce alignment	Tracer penetration, FRAP (Deff); pressure-driven permeability (κ); SHG fiber alignment	CAF-driven contraction alters geometry/flow; batch variability
Fibrin[156–158]	Angiogenic/inflammatory context; supports endothelial adhesion	Fibrinogen/thrombin ratio; crosslinking; inclusion of HA	Perfusable vascular models; permeability and transport under remodeling	Fast degradation; contraction; variable polymerization
Hyaluronic acid (HA) blends[98,159,160]	Recapitulates glycosaminoglycan-rich stroma; affects swelling and IFP	HA content; crosslinking; hyaluronidase treatments	IFP/Δp effects; diffusion hindrance; swelling	Over-swelling; undefined rheology if not crosslinked
GelMA[149,161]	Tunable mesh and stiffness; photopolymerizable	Degree of methacrylation; % GelMA; photoinitiator and light dose	Systematic Deff vs mesh-size calibration; controlled experiments	Phototoxicity; diffusion depends on curing uniformity
PEGDA[162–164]	Highly controllable and reproducible synthetic network	Crosslink density; MW; degradable linkers	Benchmark diffusion/permeability vs mesh size	Lacks native ligands unless modified; can alter cell phenotype
Matrigel (if used)[165–167]	Basement-membrane-like cues for tumor organoids	Dilution; mixing with collagen	Drug penetration in organoid contexts	Batch variability; undefined composition; not ideal for quantitative transport

Supplementary Section S5: Hydrogel materials and matrix stabilization strategies

Hydrogels form the core of ToC systems modeling desmoplastic tumor microenvironments. Natural ECM-based hydrogels, including collagen type I, fibrin, and hyaluronic acid, remain the most widely used due to their native integrin-binding motifs, proteolytic degradability, and compatibility with CAF and cancer cell remodeling programs.[113,138–141] In confined microfluidic geometries, however, fibroblast-driven contraction of collagen and fibrin gels can substantially alter matrix density, porosity, and transport properties over time.[142–144]

Several strategies have been developed to stabilize hydrogels against excessive compaction. Chemical crosslinking agents such as genipin increase network stiffness while maintaining cytocompatibility.[145,146] Interfacial anchoring approaches combine surface functionalization with covalent coupling at the gel–device interface, for example using EDC/NHS chemistry or genipin-mediated crosslinking. [145–147] Mild photochemical or click-based crosslinking methods offer spatial control over matrix stiffness with limited cytotoxicity.[148]

Synthetic and hybrid hydrogels, including polyethylene glycol (PEG)-based systems, GelMA, PEGDA, and alginate derivatives, provide improved reproducibility and tunable mechanical properties but lack native biochemical complexity.[149,150] Hybrid formulations combining synthetic backbones with natural ECM components partially reconcile tunability with biological relevance.[141,151] Phototunable and photodegradable hydrogels further enable spatial modulation of stiffness and porosity, offering experimental control over transport heterogeneity, although their application in ToC remains relatively limited.[152,153]

Supplementary Section S6: Gel confinement, anchoring, and mechanical integrity

Beyond material selection, device geometry and confinement strategies strongly influence matrix stability and transport reproducibility. Stepped-height channels and capillary-burst valve designs exploit surface tension to confine hydrogels within defined compartments while preserving perfusion pathways.[168] Continuous perfusion maintains channel patency but does not fully prevent fibroblast-driven compaction, which often necessitates additional anchoring or crosslinking strategies.[145–147,169]

Mechanical confinement and chemical anchoring act synergistically to counteract gel contraction, particularly in long-term cultures where CAF activity intensifies.[143–145] Failure to adequately stabilize the matrix can lead to uncontrolled changes in local flow paths, pressure gradients, and solute distribution, thereby obscuring biological interpretation.[143,144] Detailed reporting of anchoring strategies, confinement geometries, and perfusion conditions is therefore essential for reproducibility.

Supplementary Section S7: Measurement techniques and technical limitations

Quantifying transport in ToC systems relies on a combination of direct and indirect measurement techniques. Fluorescence recovery after photobleaching (FRAP) and fluorescence correlation spectroscopy (FCS) enable estimation of effective diffusivity but may be affected by photobleaching artefacts, limited sampling volumes, or tracer-specific biases.[52,170] Single-particle tracking (SPT) provides high spatial resolution but often employs nanoparticles larger than many therapeutic molecules, complicating extrapolation.[171]

Structural imaging modalities such as second-harmonic generation (SHG) and confocal reflectance microscopy characterize collagen architecture and alignment but do not directly measure transport.[172] Mechanical mapping approaches, including atomic force microscopy (AFM), Brillouin microscopy, and elastography, probe different mechanical regimes and spatial scales, each with distinct limitations.[116,173]

Because no single technique fully captures transport behavior, multimodal strategies combining structural imaging, mechanical mapping, direct transport assays, and computational modeling are increasingly adopted. Such integration is necessary to derive consistent estimates of effective diffusivity, permeability, and poroelastic parameters across spatial and temporal scales.

Supplementary Section S8: Reporting standards and reproducibility considerations

Transport measurements in ToC systems are highly sensitive to experimental details. Inter-laboratory studies have reported substantial variability even under nominally identical conditions, reflecting both biological heterogeneity and technical artefacts. Minor differences in gel preparation, handling, compression, or perfusion can result in order-of-magnitude differences in estimated permeability or diffusivity.

Supplementary Section S9: Practical and regulatory constraints for transport-based phenotyping

While transport-resolved tumor-on-chip (ToC) platforms provide mechanistic insight into drug accessibility, several practical and regulatory barriers currently limit their clinical deployment. To date, no ToC platform has received formal FDA clearance or CLIA certification for routine clinical use with patient samples (Clinical Laboratory Improvement Amendments). Although both the FDA and CDC are actively evaluating microphysiological systems through pilot initiatives such as the Innovative Science and Technology Approaches

for New Drugs (ISTAND) program, broader regulatory adoption remains constrained by challenges in standardization, validation, and definition of appropriate contexts of use.[174,175]

Beyond regulatory considerations, assay turnaround time remains a significant limitation for time-sensitive clinical applications. While microfluidic transport assays based on established cancer cell lines can provide interpretable results within 5–7 days,[176] workflows involving patient-derived material often require substantially longer durations. Patient-derived organoids (PDOs), typically require 2-4 weeks for establishment and maturation, and in some cases up to 6-8 weeks, which exceeds the timeframe compatible with many therapeutic decisions.[177,178]

Supplementary Section S10: Representability, success rates, and selection bias in patient-derived models

Success rates for generating patient-derived tumor cultures vary widely across tumor types and laboratories, reflecting both biological heterogeneity and technical attrition. For example, only approximately 31% of esophageal adenocarcinoma biopsies have been reported to yield stable organoid cultures.[179] A recent meta-analysis in gastric cancer reported an average success rate of approximately 66.6% across multiple studies.[180] Such variability suggests that current *in vitro* platforms may preferentially represent specific tumor subtypes, thereby introducing bias in translational studies.

In addition, prolonged *ex vivo* culture can induce phenotypic drift in both tumor and stromal compartments, progressively decoupling experimental observations from the *in vivo* state.[74,75,181] Although organoids remain valuable for cell banking, expansion, and genetic manipulation when sample material is limited, their extended culture time limits their applicability for rapid transport phenotyping. For time-sensitive applications, direct incorporation of freshly resected patient tissue into ToC systems offers a more efficient alternative, albeit with increased technical complexity and stringent quality-control requirements.

Supplementary Section S11: Extended clinical and preclinical validation examples

A growing body of evidence supports the translational relevance of transport-resolved ToC platforms across tumor entities. In an esophageal adenocarcinoma model, neoadjuvant chemotherapy responses were accurately reproduced *ex vivo* for all eight patients within 12 days, closely matching parallel clinical outcomes.[182] Comparable concordance between *in vitro* and *in vivo* responses has been reported in breast and prostate cancer tissue slice cultures, which reproduced sensitivity to cisplatin and apalutamide, respectively.[183]

Pancreatic cancer models further highlight the importance of transport limitation. Hydrogel-based PDAC tumor chips generated patient-specific drug-response profiles consistent with clinical follow-up data, demonstrating that matrix density and permeability critically modulate therapeutic efficacy.[184] Preclinical benchmarking studies reinforce these observations: irinotecan efficacy in microfluidic tumor spheroids closely matched xenograft responses (52% versus 53% growth inhibition), confirming quantitative alignment across platforms.[176] Similarly, reproducing the clinical behavior of liposomal doxorubicin (Doxil) required explicit modeling of diffusion, binding, and clearance mechanisms within tumor-mimetic chips.[115]

Collectively, these studies demonstrate that transport-based phenotypes extracted from ToC platforms can align quantitatively with *in vivo* pharmacokinetics and therapeutic outcomes when physical transport processes are explicitly accounted for.

Supplementary Section S12: Transport-based phenotyping versus molecular biomarkers

While genomic and molecular biomarkers identify intrinsic susceptibilities within tumor cells, they provide limited information regarding physical drug accessibility within the tumor microenvironment. Transport-based phenotyping complements molecular diagnostics by directly probing effective diffusivity, intrinsic permeability,

interstitial fluid pressure, and matrix stiffness, parameters that integrate stromal composition, vascular function, and mechanical stress.[51,102,185]

Clinical and preclinical studies consistently show that tumors exhibiting higher effective permeability respond more rapidly and robustly to treatment, whereas dense, transport-limiting matrices delay drug accumulation and require prolonged exposure to achieve comparable therapeutic effects.[51,102,115,176,184,185] Transport metrics therefore represent functional biomarkers of accessibility rather than molecular vulnerability.

Supplementary Section S13: Outlook for clinical translation of transport-based biomarkers

Despite increasing experimental validation, transport-based biomarkers remain at an early stage of clinical translation. Their interpretation depends on experimental context, drug physicochemical properties, and tumor architecture, and they currently lack standardized thresholds for clinical decision-making. As a result, transport phenotyping is best viewed as a stratification and hypothesis-generating tool rather than a standalone predictive assay.

Future progress will require harmonized protocols, multicenter validation studies, and clearer regulatory pathways for physical and functional biomarkers. As these challenges are addressed, transport-resolved ToC platforms may evolve into valuable companions to molecular diagnostics, particularly for desmoplastic tumors in which CAF-driven physical barriers dominate therapeutic failure.

Supplementary Section S14: Expanded matrix modulation and stromal-targeting strategies

While the main text focuses on representative examples of matrix normalization, a broader spectrum of stromal-targeting approaches has been explored preclinically. Engineered nanoparticles provide particularly refined spatial and temporal control over ECM remodeling. Photodynamic therapy has been shown to transiently activate matrix metalloproteinases through cytokine-mediated signaling, generating short-lived windows of enhanced drug penetration without permanently destabilizing tissue architecture.[186]

Hyaluronidase-functionalized nanocapsules represent another strategy, combining mechanical deformation within dense matrices with enzymatic degradation of hyaluronan. These dual-function systems synergistically improve intratumoral transport and drug penetration.[187] When coupled with pH-responsive designs, enzymatic activity can be confined to acidic tumor regions, thereby minimizing off-target effects in normal tissues.[188,189] Together, these nanoscale approaches demonstrate how localized and time-controlled ECM modulation can maximize therapeutic access while limiting systemic toxicity.

Metabolic targeting of stromal cells provides an orthogonal route to matrix modulation. Metabolically hyperactive CAFs are major contributors to ECM synthesis and stiffening. Limiting their energy supply reduces matrix deposition and softens the tumor microenvironment. Preclinical nanotherapies such as glucose-responsive L-Arg-HMON-GOx nanoparticles illustrate this concept. These systems act as glucose-responsive prodrugs: glucose oxidase catalyzes the conversion of glucose into gluconic acid and cytotoxic H_2O_2, which subsequently oxidizes L-arginine to nitric oxide.[112,190] This dual-action mechanism simultaneously depletes intratumoral glucose, generates reactive oxygen species, and releases nitric oxide, thereby suppressing stromal metabolism while inducing tumor cell death.

Despite their promise, such approaches raise safety concerns. Stromal modification may increase vascular permeability or reduce mechanical containment, potentially facilitating tumor cell dissemination.[191] These risks underscore the importance of careful patient stratification and controlled dosing strategies, particularly when combining metabolic and mechanical interventions.[192]

Supplementary Section S15: Mechanistic basis and preclinical evidence for sequential therapy

Sequential therapy approaches leverage the temporal dynamics of stromal remodeling to enhance therapeutic efficacy. Conditioning the tumor microenvironment prior to cytotoxic or immunomodulatory treatment has

repeatedly shown superior outcomes compared with simultaneous co-administration. Beyond the examples highlighted in the main text, multiple preclinical studies demonstrate that stromal reprogramming alters transport properties in a time-dependent manner, creating transient windows of enhanced accessibility.

In immunotherapy, reducing matrix stiffness or relieving physical barriers has been shown to restore infiltration of $CD8^+$ T cells into tumor cores, converting immune-excluded tumors into inflamed phenotypes. Stromal normalization enhances the efficacy of immune checkpoint blockade by facilitating immune cell access to previously inaccessible regions.[193,194] Inhibition of LOX/LOXL-mediated collagen crosslinking follows a similar principle, improving T-cell infiltration and sensitizing tumors to anti–PD-L1 therapy.[195]

Additional strategies include targeting stromal cell sialylation, which reprograms fibroblast phenotypes, relieves matrix-driven immune exclusion, and enhances cytotoxic T-cell entry.[196] Collectively, these studies highlight that the success of sequential therapy critically depends on defining the optimal therapeutic window, which is governed by the kinetics of matrix remodeling and stress redistribution rather than by drug pharmacokinetics alone.

Supplementary Section S16: Imaging biomarkers and clinical translation of transport-targeted therapies

Functional imaging modalities are increasingly integrated into clinical trials to stratify patients and monitor response to stromal-targeted therapies. Magnetic resonance elastography (MRE) provides a non-invasive measure of tumor stiffness and has demonstrated predictive value in breast cancer neoadjuvant settings.[118] Dynamic contrast-enhanced MRI (DCE-MRI) complements stiffness measurements by probing vascular function. The volume transfer constant (K^{trans}) integrates blood flow, vascular permeability, and surface area, serving as a functional surrogate for drug delivery capacity.

In pancreatic ductal adenocarcinoma, PEGPH20 treatment led to rapid increases in K^{trans}, correlating with hyaluronan depletion, vascular decompression, and improved drug delivery.[197–199] Diffusion-weighted MRI (DW-MRI) further links apparent diffusion coefficient values to cellularity and apoptotic response during treatment.[200] Ultrasound elastography has similarly been used to correlate increased stiffness with malignancy grade and to track mechanical changes during therapy. In endometrial carcinoma, combined 3D MRE and MRI measurements demonstrated that elastography-derived stiffness predicts tumor invasiveness and grade.[201,202] Despite these advances, clinical translation remains constrained by several factors: variability in imaging infrastructure and expertise, lack of standardized physical biomarker thresholds, and safety concerns associated with stromal modulation. These challenges highlight the need for harmonized imaging protocols and validated transport-related endpoints in future trials.

Supplementary Table S4: Ongoing Clinical Trials Targeting Physical Barriers in Cancer

Trial ID	Agent	Target	Cancer Type	Primary Endpoint	Status
NCT03481920[203]	PEGPH20 + Avelumab	Hyaluronidase	Chemotherapy-Resistant PDAC	Objective Response Rate (ORR) per RECIST v1.1 at 6 months	Early Phase I completed
NCT01453153[204]	PEGPH20 + Gemcitabine	Hyaluronidase	Stage IV Previously Untreated PDAC	Number of participants with a dose-limiting toxicity (DLT) during the dose-escalation phase	Phase 1B/II completed
NCT03634332[205]	PEGPH20 + Pembrolizumab	Hyaluronidase	HA High Metastatic PDAC	Progression-free survival (PFS)	Phase II recruiting
NCT05365893[206]	Losartan + FOLFIRINOX	Angiotensin II receptor	Pancreatic	Number of participants with grade ≥3 treatment-related adverse events per CTCAE v5.0 and completion of ≥4 weeks of PHL without delay to planned surgery	Phase I recruiting
NCT03563248[207]	Losartan + Nivolumab in combination with FOLFIRINOX + Radiation Therapy	Angiotensin II receptor	Localized PDAC	Rate of R0 resection	Phase II completed
NCT05077800[208]	Losartan + FOLFIRINOX + 9-Ing-41 (glycogen synthase kinase-3β inhibitor)	Angiotensin II receptor	Metastatic PDAC	PFS	Phase II recruiting
NCT02688712[209]	Galunisertib (LY2157299) + Capecitabine or Fluorouracil	TGFβ	Rectal cancer	Evaluation of pathologic response	Phase II active, not recruiting
NCT01373164[210]	Galunisertib (LY2157299) + Gemcitabine	TGFβ	Advanced PDAC	Phase 1b: Recommended Phase 2 Dose (RP2D) based on DLTs, toxicity, dose modifications, and PK; Phase 2: Overall Survival (OS) from randomization to death from any cause	Phase II completed
NCT01195415[211]	Vismodegib+ Gemcitabine Hydrochloride	Sonic Hedgehog	Advanced PDAC	Change in Median $CD44^+/CD24^+/ESA^+$ Cell Fraction (FACS) at 3 Weeks	Phase II completed
NCT02436408[212]	Vismodegib	Sonic Hedgehog	Orbital and Periocular Basal Cell Carcinoma	Proportion of Patients With Visual Assessment Weighted Score ≥21 at End of Treatment	Phase IV completed
NCT02210559[213]	Pamrevlumab (FG-3019) + Gemcitabine/nab-paclitaxel	CTGF/CCN2	Locally advanced unresectable PDAC	Incidence of Treatment-Emergent Adverse Events (TEAEs), Serious Adverse Events (SAEs) through 28 days post–last infusion or day before surgery, and Post-Resection Surgical	Phase II completed

				Complications (within 30 days post-discharge)	
NCT05482451[214]	All-trans retinoic acid + Nivolumab	Vitamin D	Refractory Pancreatic Cancer		Early Phase 1 active, not recruiting
NCT02403778[215]	All-trans retinoic acid + Ipilimumab	Vitamin D	Advanced Melanoma	Safety and Tolerability (Incidence of Adverse Events up to 2 years from enrollment), and Myeloid-Derived Suppressor Cell (MDSC) Frequency (84–130 days post–first treatment) and Suppressive Function (≥30 days post–final infusion)	Phase II completed
NCT01472198[216]	Simtuzumab (GS-6624) + Gemcitabine	LOXL2	Metastatic PDAC	PFS	Phase II completed
NCT05109052[217]	PXS-5505 + Atezolizumab and Bevacizumab	Pan-LOX	Unresectable Hepatocellular Carcinoma	Safety and Tolerability	Phase I/IIa recruiting
NCT00401570[218]	Volociximab + Gemcitabine	Integrin α5β1	Metastatic PDAC	Proportion of Patients With Confirmed Tumor Response	Phase II completed
NCT05228015[219]	IK-930	YAP/TAZ	Advanced solid tumors	Safety, Tolerability, and Dose Determination of IK-930	Phase I recruiting
NCT03727880[220]	Defactinib (VS-6063) + Pembrolizumab + Neoadjuvant and Adjuvant chemotherapy	FAK	Resectable PDAC	Pathologic complete response (pCR) rate	Phase II recruiting

Table S5 Patient-derived ToC workflow constraints for transport phenotyping

Workflow step	Key decision points	Transport-relevant QC / readouts	Common constraints
Sample acquisition & dissociation	Preserve CAF states; minimize ischemia time	Viability; CAF marker panel; initial ECM gene expression	Limited tissue; variable quality
Short-term culture / embedding	Choose ECM and confinement to preserve phenotype	Time-course Deff/κ; gel compaction; CAF activation markers	Phenotypic drift begins early; limited window
Co-culture assembly (tumor + CAF)	Patient-matched vs mixed; CAF subtype enrichment	Spatial organization; barrier emergence time; penetration depth	Scaling experiments is resource-intensive
Perturbation & sequencing	Normalization/enzyme timing; drug scheduling	Dynamic changes in Δp, Deff, κ; efficacy readouts	Temporal mismatch vs clinical months–years
Data integration	Parameter fitting; reporting standards	Model fit quality; uncertainty; reproducibility checklist	Inter-lab variance; method sensitivity

Table S6 Optional AI-assisted experimental design

AI / computational approach	What it optimizes	Use in transport phenotyping	Minimum data needed
Active learning[221,222]	Next best experiment selection	Iteratively chooses CAF composition / matrix condition / drug dosing that maximizes information gain for parameter estimation	Initial small design + readout metrics (Deff, κ, penetration depth)
Bayesian optimization[223,224]	Efficient parameter search	Finds conditions that optimize penetration or minimize barrier formation with few experiments	Objective metric + bounds; noise estimates
Surrogate modeling[225]	Fast prediction of outcomes	Learns mapping from controllable inputs (gel %, crosslinking, CAF ratio) to outputs (D_{eff}, k) for real-time planning	Moderate dataset across conditions
Deep reinforcement learning[226]	Policy for sequential interventions	Designs multi-step regimens (e.g., normalization then drug) maximizing penetration while limiting invasion	Time-series readouts; defined reward

References

1 J. Najera, M. R. Rosenberger and M. Datta, *Cancers (Basel)*, 2023, **15**, 3285.
2 K. Burke and E. Brown, *Intravital*, 2015, **3**, e984509.
3 J. Sapudom, C. D. Müller, K.-T. Nguyen, S. Martin, U. Anderegg and T. Pompe, *Gels*, 2020, **6**, 33.
4 T. Imamura, H. Iguchi, T. Manabe, G. Ohshio, T. Yoshimura, Z. H. Wang, H. Suwa, S. Ishigami and M. Imamura, *Pancreas*, 1995, **11**, 357–364.
5 B. Hinz, G. Celetta, J. J. Tomasek, G. Gabbiani and C. Chaponnier, *MBoC*, 2001, **12**, 2730–2741.
6 J. Winkler, A. Abisoye-Ogunniyan, K. J. Metcalf and Z. Werb, *Nat Commun*, 2020, **11**, 5120.
7 P. Tenti and L. Vannucci, *Cancer Immunol Immunother*, 2019, **69**, 223–235.
8 K. Chen, M. Xu, F. Lu and Y. He, *Tissue Eng Regen Med*, 2023, **20**, 661–670.
9 R. L. Blackmon, R. Sandhu, B. S. Chapman, P. Casbas-Hernandez, J. B. Tracy, M. A. Troester and A. L. Oldenburg, *Biophys J*, 2016, **110**, 1858–1868.
10 J. R. Staunton, B. L. Doss, S. Lindsay and R. Ros, *Sci Rep*, 2016, **6**, 19686.
11 H. Haslene-Hox, E. Oveland, K. Woie, H. B. Salvesen, O. Tenstad and H. Wiig, *American Journal of Physiology-Heart and Circulatory Physiology*, 2015, **308**, H18–H28.
12 A. Avendano, J. J. Chang, M. G. Cortes-Medina, A. J. Seibel, B. R. Admasu, C. M. Boutelle, A. R. Bushman, A. A. Garg, C. M. DeShetler, S. L. Cole and J. W. Song, *ACS Biomater Sci Eng*, 2020, **6**, 1408–1417.
13 C. S. Vidmar, M. Bazzi and V. K. Lai, *Journal of the Mechanical Behavior of Biomedical Materials*, 2022, **128**, 105107.
14 V. Serpooshan, M. Julien, O. Nguyen, H. Wang, A. Li, N. Muja, J. E. Henderson and S. N. Nazhat, *Acta Biomater*, 2010, **6**, 3978–3987.
15 H. Salavati, P. Pullens, C. Debbaut and W. Ceelen, *Bioeng Transl Med*, 2023, **9**, e10617.
16 L. Cords, S. Tietscher, T. Anzeneder, C. Langwieder, M. Rees, N. de Souza and B. Bodenmiller, *Nat Commun*, 2023, **14**, 4294.
17 S. Piccolo, T. Panciera, P. Contessotto and M. Cordenonsi, *Nat Cancer*, 2023, **4**, 9–26.
18 T. Panciera, L. Azzolin, M. Cordenonsi and S. Piccolo, *Nat Rev Mol Cell Biol*, 2017, **18**, 758–770.
19 N. Wang, *J Phys D Appl Phys*, 2017, **50**, 233002.
20 I. Dasgupta and D. McCollum, *Journal of Biological Chemistry*, 2019, **294**, 17693–17706.
21 D. Y. Zhang and S. L. Friedman, *Hepatology*, 2012, **56**, 769–775.
22 S. Ramanujan, A. Pluen, T. D. McKee, E. B. Brown, Y. Boucher and R. K. Jain, *Biophysical Journal*, 2002, **83**, 1650–1660.
23 A. E. Kamholz, B. H. Weigl, B. A. Finlayson and P. Yager, *Anal Chem*, 1999, **71**, 5340–5347.
24 N. R. Richbourg and N. A. Peppas, *Macromolecules*, 2021, **54**, 10477–10486.
25 A. E. Kamholz and P. Yager, *Sensors and Actuators B: Chemical*, 2002, **82**, 117–121.
26 E. Häusler, P. Domagalski, M. Ottens and A. Bardow, *Chemical Engineering Science*, 2012, **72**, 45–50.
27 M. A. K. Tolentino, E. Y. Du, G. Silvani, E. Pandzic, K. A. Kilian and J. J. Gooding, *Adv Healthc Mater*, 2025, **14**, 2500658.
28 A. Pluen, Y. Boucher, S. Ramanujan, T. D. McKee, T. Gohongi, E. di Tomaso, E. B. Brown, Y. Izumi, R. B. Campbell, D. A. Berk and R. K. Jain, *Proceedings of the National Academy of Sciences*, 2001, **98**, 4628–4633.
29 C. F. Buchanan, E. E. Voigt, C. S. Szot, J. W. Freeman, P. P. Vlachos and M. N. Rylander, *Tissue Eng Part C Methods*, 2014, **20**, 64–75.
30 W. J. Polacheck, J. L. Charest and R. D. Kamm, *Proc Natl Acad Sci U S A*, 2011, **108**, 11115–11120.
31 X. Lu, Y. Zhao and D. J. C. Dennis, *Phys. Rev. Fluids*, 2018, **3**, 104202.
32 W. Song and D. Psaltis, *Biomicrofluidics*, 2011, **5**, 044110-044110–11.
33 R. Lindken, M. Rossi, S. Große and J. Westerweel, *Lab Chip*, 2009, **9**, 2551–2567.
34 M. D. A. Norman, S. A. Ferreira, G. M. Jowett, L. Bozec and E. Gentleman, *Nat Protoc*, 2021, **16**, 2418–2449.
35 Y. Hu, X. Zhao, J. J. Vlassak and Z. Suo, *Appl. Phys. Lett.*, 2010, **96**, 121904.
36 D. Caccavo, G. Lamberti and A. A. Barba, *European Journal of Pharmaceutics and Biopharmaceutics*, 2020, **152**, 299–306.
37 M. Lekka, K. Gnanachandran, A. Kubiak, T. Zieliński and J. Zemła, *Micron*, 2021, **150**, 103138.
38 M. H. Esteki, A. A. Alemrajabi, C. M. Hall, G. K. Sheridan, M. Azadi and E. Moeendarbary, *Acta Biomater*, 2020, **102**, 138–148.
39 F. C. Fischer, C. Abele, S. T. J. Droge, L. Henneberger, M. König, R. Schlichting, S. Scholz and B. I. Escher, *Chem Res Toxicol*, 2018, **31**, 646–657.
40 B. J. van Meer, H. de Vries, K. S. A. Firth, J. van Weerd, L. G. J. Tertoolen, H. B. J. Karperien, P. Jonkheijm, C. Denning, A. P. IJzerman and C. L. Mummery, *Biochemical and Biophysical Research Communications*, 2017, **482**, 323–328.
41 T. E. Winkler and A. Herland, *ACS Appl. Mater. Interfaces*, 2021, **13**, 45161–45174.
42 G. A. Busby, M. H. Grant, S. P. Mackay and P. E. Riches, *J Biomech*, 2013, **46**, 837–840.
43 Y. Qin, K. Yue, X. Yu, Y. You, C. Yang and X. Zhang, *Bioengineering (Basel)*, 2025, **12**, 429.
44 O. Degerstedt, P. O'Callaghan, A. L. Clavero, J. Gråsjö, O. Eriksson, E. Sjögren, P. Hansson, F. Heindryckx, J. Kreuger and H. Lennernäs, *Drug Deliv Transl Res*, 2024, **14**, 970–983.
45 P. W. Sweeney, A. d'Esposito, S. Walker-Samuel and R. J. Shipley, *PLoS Comput Biol*, 2019, **15**, e1006751.
46 X. Zheng, K. Zhao, T. Jackson and J. Lowengrub, *J. Math. Biol.*, 2022, **85**, 5.
47 M. A. Biot, *J. Appl. Phys.*, 1941, **12**, 155–164.
48 R. K. Jain, J. D. Martin and T. Stylianopoulos, *Annu Rev Biomed Eng*, 2014, **16**, 321–346.

49 M. A. Biot, *J. Appl. Phys.*, 1955, **26**, 182–185.
50 F. Moradi Kashkooli, M. Soltani, M. M. Momeni and A. Rahmim, *Front Oncol*, 2021, **11**, 655781.
51 P. A. Netti, L. T. Baxter, Y. Boucher, R. Skalak and R. K. Jain, *Cancer Res*, 1995, **55**, 5451–5458.
52 H. Ishikawa-Ankerhold, R. Ankerhold and G. Drummen, in *eLS*, John Wiley & Sons, Ltd, 2014.
53 J. J. Mack, K. Youssef, O. D. V. Noel, M. P. Lake, A. Wu, M. L. Iruela-Arispe and L.-S. Bouchard, *Biomaterials*, 2013, **34**, 1980–1986.
54 C. Nicholson and E. Syková, *Trends in Neurosciences*, 1998, **21**, 207–215.
55 H. A. Leddy, M. A. Haider and F. Guilak, *Biophys J*, 2006, **91**, 311–316.
56 K. Hashlamoun, Z. Abusara, A. Ramírez-Torres, A. Grillo, W. Herzog and S. Federico, *Biomech Model Mechanobiol*, 2020, **19**, 2397–2412.
57 L. T. Baxter and R. K. Jain, *Microvasc Res*, 1989, **37**, 77–104.
58 R. K. Jain, *Annu Rev Biomed Eng*, 1999, **1**, 241–263.
59 E. Axpe, D. Chan, G. S. Offeddu, Y. Chang, D. Merida, H. L. Hernandez and E. A. Appel, *Macromolecules*, 2019, **52**, 6889–6897.
60 M. H. Hettiaratchi, A. Schudel, T. Rouse, A. J. García, S. N. Thomas, R. E. Guldberg and T. C. McDevitt, *APL Bioeng*, 2018, **2**, 026110.
61 A. K. Miri, H. G. Hosseinabadi, B. Cecen, S. Hassan and Y. S. Zhang, *Acta Biomater*, 2018, **77**, 38–47.
62 G. S. Offeddu, E. Axpe, B. A. C. Harley and M. L. Oyen, *AIP Adv*, 2018, **8**, 105006.
63 S. S. Jang, W. A. Goddard and M. Y. S. Kalani, *J. Phys. Chem. B*, 2007, **111**, 1729–1737.
64 M. P. Gagnon, P. Bissonnette, L.-M. Deslandes, B. Wallendorff and J.-Y. Lapointe, *Biophysical Journal*, 2004, **86**, 125–133.
65 J. Wang, A. D. Gonzalez and V. M. Ugaz, *Advanced Materials*, 2008, **20**, 4482–4489.
66 C. Xue, Y. Huang, X. Zheng and G. Hu, *J. Phys. Chem. Lett.*, 2022, **13**, 10612–10620.
67 G. J. Laurent, R. C. Chambers, M. R. Hill and R. J. McAnulty, *Biochem Soc Trans*, 2007, **35**, 647–651.
68 S. Knoedler, S. Broichhausen, R. Guo, R. Dai, L. Knoedler, M. Kauke-Navarro, F. Diatta, B. Pomahac, H.-G. Machens, D. Jiang and Y. Rinkevich, *Front Immunol*, 2023, **14**, 1233800.
69 F. Kawecki, M. Gluais, S. Claverol, N. Dusserre, T. McAllister and N. L'Heureux, *Biomater Sci*, 2022, **10**, 3935–3950.
70 D. K. Logsdon, G. F. Beeghly and J. M. Munson, *Cell Mol Bioeng*, 2017, **10**, 463–481.
71 G. Biffi, T. E. Oni, B. Spielman, Y. Hao, E. Elyada, Y. Park, J. Preall and D. A. Tuveson, *Cancer Discov*, 2019, **9**, 282–301.
72 T. Zhang, Y. Ren, P. Yang, J. Wang and H. Zhou, *Cell Death Dis*, 2022, **13**, 897.
73 D. Öhlund, A. Handly-Santana, G. Biffi, E. Elyada, A. S. Almeida, M. Ponz-Sarvise, V. Corbo, T. E. Oni, S. A. Hearn, E. J. Lee, I. I. C. Chio, C.-I. Hwang, H. Tiriac, L. A. Baker, D. D. Engle, C. Feig, A. Kultti, M. Egeblad, D. T. Fearon, J. M. Crawford, H. Clevers, Y. Park and D. A. Tuveson, *J Exp Med*, 2017, **214**, 579–596.
74 S. González-Lana, T. Randelovic, J. Ciriza, M. López-Valdeolivas, R. Monge, C. Sánchez-Somolinos and I. Ochoa, *Lab Chip*, 2023, **23**, 2434–2446.
75 L. Mathieson, P. Jones, L. Koppensteiner, L. Neilson, D. A. Dorward, R. O'Connor and A. R. Akram, *BJC Rep*, 2025, **3**, 50.
76 M. Soltani and P. Chen, *PLoS One*, 2011, **6**, e20344.
77 M. Sefidgar, M. Soltani, K. Raahemifar, M. Sadeghi, H. Bazmara, M. Bazargan and M. Mousavi Naeenian, *Microvascular Research*, 2015, **99**, 43–56.
78 R. A. A, V. A. A, A. A. A and D. K. V, *St. Petersburg Polytechnic University Journal: Physics and Mathematics*, 2023, **64**, 253–259.
79 B. Wirthl, J. Kremheller, B. A. Schrefler and W. A. Wall, *PLOS ONE*, 2020, **15**, e0228443.
80 R. P. Chilcott, N. Barai, A. E. Beezer, S. I. Brain, M. B. Brown, A. L. Bunge, S. E. Burgess, S. Cross, C. H. Dalton, M. Dias, A. Farinha, B. C. Finnin, S. J. Gallagher, D. M. Green, H. Gunt, R. L. Gwyther, C. M. Heard, C. A. Jarvis, F. Kamiyama, G. B. Kasting, E. E. Ley, S. T. Lim, G. S. McNaughton, A. Morris, M. H. Nazemi, M. A. Pellett, J. Du Plessis, Y. S. Quan, S. L. Raghavan, M. Roberts, W. Romonchuk, C. S. Roper, D. Schenk, L. Simonsen, A. Simpson, B. D. Traversa, L. Trottet, A. Watkinson, S. C. Wilkinson, F. M. Williams, A. Yamamoto and J. Hadgraft, *J Pharm Sci*, 2005, **94**, 632–638.
81 C. L. Pires and M. J. Moreno, *Membranes*, DOI:10.3390/membranes14070157.
82 P. P. Adiseshaiah, R. M. Crist, S. S. Hook and S. E. McNeil, *Nat Rev Clin Oncol*, 2016, **13**, 750–765.
83 G. S. Offeddu, E. Cambria, S. E. Shelton, K. Haase, Z. Wan, L. Possenti, H. T. Nguyen, M. R. Gillrie, D. Hickman, C. G. Knutson and R. D. Kamm, *Advanced Science*, 2024, **11**, 2402757.
84 L. Miao, C. M. Lin and L. Huang, *J Control Release*, 2015, **219**, 192–204.
85 M. Binnewies, E. W. Roberts, K. Kersten, V. Chan, D. F. Fearon, M. Merad, L. M. Coussens, D. I. Gabrilovich, S. Ostrand-Rosenberg, C. C. Hedrick, R. H. Vonderheide, M. J. Pittet, R. K. Jain, W. Zou, T. K. Howcroft, E. C. Woodhouse, R. A. Weinberg and M. F. Krummel, *Nat Med*, 2018, **24**, 541–550.
86 Y. Ju, D. Xu, M. Liao, Y. Sun, W. Bao, F. Yao and L. Ma, *npj Precis. Onc.*, 2024, **8**, 199.
87 S. Azadi, H. Aboulkheyr Es, S. Razavi Bazaz, J. P. Thiery, M. Asadnia and M. Ebrahimi Warkiani, *Biochimica et Biophysica Acta (BBA) - Molecular Cell Research*, 2019, **1866**, 118526.
88 C. Dextras, M. Dashnyam, L. A. M. Griner, J. Sundaresan, B. Chim, Z. Yu, S. Vodnala, C.-C. R. Lee, X. Hu, N. Southall, J. J. Marugan, A. Jadhav, N. P. Restifo, N. Acquavella, M. Ferrer and A. Singh, *Sci Rep*, 2020, **10**, 5688.
89 J. A. Joyce and D. T. Fearon, *Science*, 2015, **348**, 74–80.
90 J. L. Farlow, J. C. Brenner, Y. L. Lei and S. B. Chinn, *Oral Oncol*, 2021, **120**, 105420.
91 L. A. Shuman Moss, S. Jensen-Taubman and W. G. Stetler-Stevenson, *The American Journal of Pathology*, 2012, **181**, 1895–1899.

92 S. Ricard-Blum and S. D. Vallet, *Front Pharmacol*, 2016, **7**, 11.
93 T. Salo, M. Sutinen, E. Hoque Apu, E. Sundquist, N. K. Cervigne, C. E. de Oliveira, S. U. Akram, S. Ohlmeier, F. Suomi, L. Eklund, P. Juusela, P. Åström, C. C. Bitu, M. Santala, K. Savolainen, J. Korvala, A. F. Paes Leme and R. D. Coletta, *BMC Cancer*, 2015, **15**, 981.
94 S. Murty, T. Gilliland, P. Qiao, T. Tabtieng, E. Higbee, A. Al Zaki, E. Puré and A. Tsourkas, *Part Part Syst Charact*, 2014, **31**, 1307–1312.
95 A. Zinger, L. Koren, O. Adir, M. Poley, M. Alyan, Z. Yaari, N. Noor, N. Krinsky, A. Simon, H. Gibori, M. Krayem, Y. Mumblat, S. Kasten, S. Ofir, E. Fridman, N. Milman, M. M. Lübtow, L. Liba, J. Shklover, J. Shainsky-Roitman, Y. Binenbaum, D. Hershkovitz, Z. Gil, T. Dvir, R. Luxenhofer, R. Satchi-Fainaro and A. Schroeder, *ACS Nano*, 2019, **13**, 11008–11021.
96 C. B. Thompson, H. M. Shepard, P. M. O'Connor, S. Kadhim, P. Jiang, R. J. Osgood, L. H. Bookbinder, X. Li, B. J. Sugarman, R. J. Connor, S. Nadjsombati and G. I. Frost, *Mol Cancer Ther*, 2010, **9**, 3052–3064.
97 A. Orimo, P. B. Gupta, D. C. Sgroi, F. Arenzana-Seisdedos, T. Delaunay, R. Naeem, V. J. Carey, A. L. Richardson and R. A. Weinberg, *Cell*, 2005, **121**, 335–348.
98 P. P. Provenzano, C. Cuevas, A. E. Chang, V. K. Goel, D. D. Von Hoff and S. R. Hingorani, *Cancer Cell*, 2012, **21**, 418–429.
99 J. Ferruzzi, M. Sun, A. Gkousioudi, A. Pilvar, D. Roblyer, Y. Zhang and M. H. Zaman, *Sci Rep*, 2019, **9**, 17151.
100 B. Diop-Frimpong, V. P. Chauhan, S. Krane, Y. Boucher and R. K. Jain, *Proceedings of the National Academy of Sciences*, 2011, **108**, 2909–2914.
101 T. Stylianopoulos and R. K. Jain, *Proceedings of the National Academy of Sciences*, 2013, **110**, 18632–18637.
102 T. Stylianopoulos, J. D. Martin, V. P. Chauhan, S. R. Jain, B. Diop-Frimpong, N. Bardeesy, B. L. Smith, C. R. Ferrone, F. J. Hornicek, Y. Boucher, L. L. Munn and R. K. Jain, *Proc Natl Acad Sci U S A*, 2012, **109**, 15101–15108.
103 R. K. Jain and T. Stylianopoulos, *Nat Rev Clin Oncol*, 2010, **7**, 653–664.
104 J. Cacheux, J. Ordonez-Miranda, A. Bancaud, L. Jalabert, D. Alcaide, M. Nomura and Y. T. Matsunaga, *Science Advances*, 2023, **9**, eadf9775.
105 K. R. Levental, H. Yu, L. Kass, J. N. Lakins, M. Egeblad, J. T. Erler, S. F. T. Fong, K. Csiszar, A. Giaccia, W. Weninger, M. Yamauchi, D. L. Gasser and V. M. Weaver, *Cell*, 2009, **139**, 891–906.
106 J. Prakash and Y. Shaked, *Cancer Discov*, 2024, **14**, 1375–1388.
107 T. R. Cox, *Nat Rev Cancer*, 2021, **21**, 217–238.
108 I. Calejo, M. A. Heinrich, G. Zambito, L. Mezzanotte, J. Prakash and L. Moreira Teixeira, *Adv Exp Med Biol*, 2022, **1379**, 171–203.
109 T. Meynard, F. Royer, R. Houssier, O. Bajeux, S. Paget, F. Lahdaoui, A. M. Valdivia, N. Maubon, J. Vicogne, I. V. Seuningen and V. Senez, *Lab Chip*, 2025, **25**, 4119–4137.
110 A. Sontheimer-Phelps, B. A. Hassell and D. E. Ingber, *Nat Rev Cancer*, 2019, **19**, 65–81.
111 W. Zhan, M. Alamer and X. Y. Xu, *Advanced Drug Delivery Reviews*, 2018, **132**, 81–103.
112 W. Fan, N. Lu, P. Huang, Y. Liu, Z. Yang, S. Wang, G. Yu, Y. Liu, J. Hu, Q. He, J. Qu, T. Wang and X. Chen, *Angew Chem Int Ed Engl*, 2017, **56**, 1229–1233.
113 J.-H. Lee, S.-K. Kim, I. A. Khawar, S.-Y. Jeong, S. Chung and H.-J. Kuh, *J Exp Clin Cancer Res*, 2018, **37**, 4.
114 Z. Qi, L. Xu, Y. Xu, J. Zhong, A. Abedini, X. Cheng and D. Sinton, *Lab Chip*, 2018, **18**, 3872–3880.
115 B. J. Toley, Z. T. Lovatt, J. L. Harrington and N. S. Forbes, *Integr Biol (Camb)*, 2013, **5**, 1184–1196.
116 K. J. Glaser, A. Manduca and R. L. Ehman, *J Magn Reson Imaging*, 2012, **36**, 10.1002/jmri.23597.
117 M. J. Paszek, N. Zahir, K. R. Johnson, J. N. Lakins, G. I. Rozenberg, A. Gefen, C. A. Reinhart-King, S. S. Margulies, M. Dembo, D. Boettiger, D. A. Hammer and V. M. Weaver, *Cancer Cell*, 2005, **8**, 241–254.
118 A. P. Sinha, P. Jurrius, A.-S. van Schelt, O. Darwish, B. Shifa, G. Annio, Z. Peterson, H. Jeffery, K. Welsh, A. Metafa, J. Spence, A. Kothari, H. Hamed, G. Bitsakou, V. Karydakis, M. Thorat, E. Shaari, A. Sever, A. Rigg, T. Ng, S. Pinder, R. Sinkus and A. Purushotham, *Radiology: Imaging Cancer*, 2025, **7**, e240138.
119 T. Stylianopoulos, L. L. Munn and R. K. Jain, *Trends in Cancer*, 2018, **4**, 292–319.
120 M. Kalli and T. Stylianopoulos, *Front Oncol*, 2018, **8**, 55.
121 M. W. Toepke and D. J. Beebe, *Lab Chip*, 2006, **6**, 1484–1486.
122 K. J. Regehr, M. Domenech, J. T. Koepsel, K. C. Carver, S. J. Ellison-Zelski, W. L. Murphy, L. A. Schuler, E. T. Alarid and D. J. Beebe, *Lab Chip*, 2009, **9**, 2132–2139.
123 K. Giri and C.-W. Tsao, *Micromachines*, 2022, **13**, 486.
124 E. Gencturk, S. Mutlu and K. O. Ulgen, *Biomicrofluidics*, 2017, **11**, 051502.
125 S. Hernández-Hatibi, P. E. Guerrero, J. M. García-Aznar and E. García-Gareta, *Biomacromolecules*, 2024, **25**, 5169–5180.
126 M. Dabaghi, S. Shahriari, N. Saraei, K. Da, A. Chandiramohan, P. R. Selvaganapathy and J. A. Hirota, *Micromachines (Basel)*, 2021, **12**, 132.
127 D. Duleba, S. Denuga and R. P. Johnson, *Physical Chemistry Chemical Physics*, 2024, **26**, 15452–15460.
128 R. G. Rodrigues, P. G. M. Condelipes, R. R. Rosa, V. Chu and J. P. Conde, *Micromachines (Basel)*, 2023, **14**, 1837.
129 M. J. Lerman, J. Lembong, S. Muramoto, G. Gillen and J. P. Fisher, *Tissue Eng Part B Rev*, 2018, **24**, 359–372.
130 K. T. L. Trinh, D. A. Thai, W. R. Chae and N. Y. Lee, *ACS Omega*, 2020, **5**, 17396–17404.
131 D. Sticker, R. Geczy, U. O. Häfeli and J. P. Kutter, *ACS Appl. Mater. Interfaces*, 2020, **12**, 10080–10095.
132 S. Aralekallu, R. Boddula and V. Singh, *Materials & Design*, 2023, **225**, 111517.
133 A.-G. Niculescu, C. Chircov, A. C. Bîrcă and A. M. Grumezescu, *Int J Mol Sci*, 2021, **22**, 2011.
134 H. B. Musgrove, S. R. Cook and R. R. Pompano, *ACS Appl Bio Mater*, 2023, **6**, 3079–3083.
135 D. Kim and A. E. Herr, *Biomicrofluidics*, 2013, **7**, 041501.
136 S. E. Park, A. Georgescu, J. M. Oh, K. W. Kwon and D. Huh, *ACS Appl Mater Interfaces*, 2019, **11**, 23919–23925.

137 H. B. Musgrove, M. A. Catterton and R. R. Pompano, *Anal Chim Acta*, 2022, **1209**, 339842.
138 Q. Xu, J. E. Torres, M. Hakim, P. M. Babiak, P. Pal, C. M. Battistoni, M. Nguyen, A. Panitch, L. Solorio and J. C. Liu, *Mater Sci Eng R Rep*, 2021, **146**, 100641.
139 L. Rijns, M. G. T. A. Rutten, A. F. Vrehen, A. A. Aldana, M. B. Baker and P. Y. W. Dankers, *Nanoscale*, 2024, **16**, 16290–16312.
140 J. Jeong, N. J. Frohberg, E. Zhou, T. Sulchek and P. Qiu, *PLoS One*, 2018, **13**, e0192463.
141 E. A. Aisenbrey and W. L. Murphy, *Nat Rev Mater*, 2020, **5**, 539–551.
142 E. Bell, B. Ivarsson and C. Merrill, *Proc Natl Acad Sci U S A*, 1979, **76**, 1274–1278.
143 M. E. Smithmyer, L. A. Sawicki and A. M. Kloxin, *Biomater Sci*, 2014, **2**, 634–650.
144 M. Horie, A. Saito, Y. Yamaguchi, M. Ohshima and T. Nagase, *J Vis Exp*, 2015, 52469.
145 D. Le Manach, R. Kowsari-Esfahan, E. Reszczyńska, P. Nghe and M. Nees, *bioRxiv*, 2025, 2025.07.03.662913.
146 Y. Yu, S. Xu, S. Li and H. Pan, *Biomater. Sci.*, 2021, **9**, 1583–1597.
147 K. Nam, T. Kimura and A. Kishida, *Macromolecular Bioscience*, 2008, **8**, 32–37.
148 G. S. Major, H. Joukhdar, Y. S. Choi, J. Rnjak-Kovacina, S. G. Wise, L. A. Ju, T. R. Cox, C. Xu, G. C. Yeo, J. L. Young and K. S. Lim, *Cell Reports Physical Science*, 2025, **6**, 102366.
149 K. M. Park, D. Lewis and S. Gerecht, *Annu Rev Biomed Eng*, 2017, **19**, 109–133.
150 S. Ullah and X. Chen, *Applied Materials Today*, 2020, **20**, 100656.
151 I. G. Mercer, K. Yu, A. J. Devanny, M. B. Gordon and L. J. Kaufman, *Acta Biomaterialia*, 2024, **187**, 242–252.
152 J. E. Ortiz-Cárdenas, J. M. Zatorski, A. Arneja, A. N. Montalbine, J. M. Munson, C. J. Luckey and R. R. Pompano, *Organs-on-a-Chip*, 2022, **4**, 100018.
153 P. J. LeValley, M. W. Tibbitt, B. Noren, P. Kharkar, A. M. Kloxin, K. S. Anseth, M. Toner and J. Oakey, *Colloids Surf B Biointerfaces*, 2019, **174**, 483–492.
154 N. I. Nissen, M. Karsdal and N. Willumsen, *J Exp Clin Cancer Res*, 2019, **38**, 115.
155 F. Calvo, N. Ege, A. Grande-Garcia, S. Hooper, R. P. Jenkins, S. I. Chaudhry, K. Harrington, P. Williamson, E. Moeendarbary, G. Charras and E. Sahai, *Nat Cell Biol*, 2013, **15**, 10.1038/ncb2756.
156 F. Del Bufalo, T. Manzo, V. Hoyos, S. Yagyu, I. Caruana, J. Jacot, O. Benavides, D. Rosen and M. K. Brenner, *Biomaterials*, 2016, **84**, 76–85.
157 M. Yamauchi, T. H. Barker, D. L. Gibbons and J. M. Kurie, *J Clin Invest*, **128**, 16–25.
158 H. C. Kwaan and P. F. Lindholm, *Semin Thromb Hemost*, 2019, **45**, 413–422.
159 P. P. Provenzano and S. R. Hingorani, *Br J Cancer*, 2013, **108**, 1–8.
160 J. B. McCarthy, D. El-Ashry and E. A. Turley, *Front. Cell Dev. Biol.*, DOI:10.3389/fcell.2018.00048.
161 B. Huang, X. Wei, K. Chen, L. Wang and M. Xu, *Int J Bioprint*, 2023, **9**, 676.
162 J. R. Choi, K. W. Yong, J. Y. Choi and A. C. Cowie, *BioTechniques*, 2019, **66**, 40–53.
163 R. R. Katz and J. L. West, *Cancers (Basel)*, 2022, **14**, 1225.
164 K. Fernando, L. Gek Kwang, J. T. Chin Lim and E. L. Shan Fong, *Biomaterials Science*, 2021, **9**, 2362–2383.
165 M. T. Kozlowski, C. J. Crook and H. T. Ku, *Commun Biol*, 2021, **4**, 1387.
166 L. Wolff and S. Hendrix, *Adv Sci (Weinh)*, 2025, **12**, e08734.
167 C. S. Hughes, L. M. Postovit and G. A. Lajoie, *Proteomics*, 2010, **10**, 1886–1890.
168 S.-Y. Jeong, J.-H. Lee, Y. Shin, S. Chung and H.-J. Kuh, *PLoS One*, 2016, **11**, e0159013.
169 A. Shakeri, S. Khan and T. F. Didar, *Lab on a Chip*, 2021, **21**, 3053–3075.
170 J. Li, C. Dong and J. Ren, *TrAC Trends in Analytical Chemistry*, 2017, **89**, 181–189.
171 M. Kawai, H. Higuchi, M. Takeda, Y. Kobayashi and N. Ohuchi, *Breast Cancer Res*, 2009, **11**, R43.
172 X. Chen, O. Nadiarynkh, S. Plotnikov and P. J. Campagnola, *Nat Protoc*, 2012, **7**, 654–669.
173 T. Sun, H. Zhao, L. Hu, X. Shao, Z. Lu, Y. Wang, P. Ling, Y. Li, K. Zeng and Q. Chen, *Acta Pharmaceutica Sinica B*, 2024, **14**, 2428–2446.
174 L. R. Avula and P. Grodzinski, *Front. Lab Chip Technol.*, DOI:10.3389/frlct.2024.1487377.
175 N. Isoherranen, R. Madabushi and S.-M. Huang, *Clinical and Translational Science*, 2019, **12**, 113–121.
176 T. Petreus, E. Cadogan, G. Hughes, A. Smith, V. Pilla Reddy, A. Lau, M. J. O'Connor, S. Critchlow, M. Ashford and L. Oplustil O'Connor, *Commun Biol*, 2021, **4**, 1001.
177 T. Tan, D. Mouradov, P. Gibbs and O. M. Sieber, *STAR Protoc*, 2024, **5**, 103090.
178 S. Bose, H. Clevers and X. Shen, *Med*, 2021, **2**, 1011–1026.
179 X. Li, H. E. Francies, M. Secrier, J. Perner, A. Miremadi, N. Galeano-Dalmau, W. J. Barendt, L. Letchford, G. M. Leyden, E. K. Goffin, A. Barthorpe, H. Lightfoot, E. Chen, J. Gilbert, A. Noorani, G. Devonshire, L. Bower, A. Grantham, S. MacRae, N. Grehan, D. C. Wedge, R. C. Fitzgerald and M. J. Garnett, *Nat Commun*, 2018, **9**, 2983.
180 K.-L. Jiang, X.-X. Wang, X.-J. Liu, L.-K. Guo, Y.-Q. Chen, Q.-L. Jia, K.-M. Yang and J.-H. Ling, *World J Gastrointest Oncol*, 2024, **16**, 1626–1646.
181 K. Gorshkov, C. Z. Chen, R. E. Marshall, N. Mihatov, Y. Choi, D.-T. Nguyen, N. Southall, K. G. Chen, J. K. Park and W. Zheng, *Drug Discovery Today*, 2019, **24**, 272–278.
182 S. Pal, E. Shimshoni, S. F. Torres, M. Kong, K. Tai, V. Sangwan, N. Bertos, S. D. Bailey, J. Bérubé, D. E. Ingber and L. Ferri, *Journal of Translational Medicine*, 2025, **23**, 577.
183 S. Chakrabarty, W. F. Quiros-Solano, M. M. P. Kuijten, B. Haspels, S. Mallya, C. S. Y. Lo, A. Othman, C. Silvestri, A. van de Stolpe, N. Gaio, H. Odijk, M. van de Ven, C. M. A. de Ridder, W. M. van Weerden, J. Jonkers, R. Dekker, N. Taneja, R. Kanaar and D. C. van Gent, *Cancer Res*, 2022, **82**, 510–520.
184 T. Song, H. Zhang, Z. Luo, L. Shang and Y. Zhao, *Adv Sci (Weinh)*, 2023, **10**, e2206004.
185 R. K. Jain, *Sci Am*, 1994, **271**, 58–65.
186 S. Karrer, A. K. Bosserhoff, P. Weiderer, M. Landthaler and R. -M. Szeimies, *Br J Dermatol*, 2004, **151**, 776–783.

187 W. Lu, Y. Li, X. Zhang, N. Wang, D. Chen, Y. Zhao, G. Li, X. Shi, X. Ma, X. Su, F. Wang, C. Shu and K. Chen, *Journal of Nanobiotechnology*, 2024, **22**, 734.
188 A. A. Kale and V. P. Torchilin, in *Liposomes: Methods and Protocols, Volume 1: Pharmaceutical Nanocarriers*, ed. V. Weissig, Humana Press, Totowa, NJ, 2010, pp. 213–242.
189 H. Wang, X. Han, Z. Dong, J. Xu, J. Wang and Z. Liu, *Advanced Functional Materials*, 2019, **29**, 1902440.
190 N. Niu, X. Shen, Z. Wang, Y. Chen, Y. Weng, F. Yu, Y. Tang, P. Lu, M. Liu, L. Wang, Y. Sun, M. Yang, B. Shen, J. Jin, Z. Lu, K. Jiang, Y. Shi and J. Xue, *Cancer Cell*, 2024, **42**, 869-884.e9.
191 T. Tomita, M. Kato and S. Hiratsuka, *Cancer Sci*, 2021, **112**, 2966–2974.
192 S. R. Hingorani, L. Zheng, A. J. Bullock, T. E. Seery, W. P. Harris, D. S. Sigal, F. Braiteh, P. S. Ritch, M. M. Zalupski, N. Bahary, P. E. Oberstein, A. Wang-Gillam, W. Wu, D. Chondros, P. Jiang, S. Khelifa, J. Pu, C. Aldrich and A. E. Hendifar, *JCO*, 2018, **36**, 359–366.
193 J. A. Grout, P. Sirven, A. M. Leader, S. Maskey, E. Hector, I. Puisieux, F. Steffan, E. Cheng, N. Tung, M. Maurin, R. Vaineau, L. Karpf, M. Plaud, A.-L. Bègue, K. Ganesh, J. Mesple, M. Casanova-Acebes, A. Tabachnikova, S. Keerthivasan, A. Lansky, J. L. Bérichel, L. Walker, A. H. Rahman, S. Gnjatic, N. Girard, M. Lefèvre, D. Damotte, J. Adam, J. C. Martin, A. Wolf, R. M. Flores, M. B. Beasley, R. Pradhan, S. Müller, T. U. Marron, S. J. Turley, M. Merad, E. Kenigsberg and H. Salmon, *Cancer Discov*, 2022, **12**, 2606–2625.
194 L. Jenkins, U. Jungwirth, A. Avgustinova, M. Iravani, A. Mills, S. Haider, J. Harper and C. M. Isacke, *Cancer Res*, 2022, **82**, 2904–2917.
195 D. H. Peng, B. L. Rodriguez, L. Diao, L. Chen, J. Wang, L. A. Byers, Y. Wei, H. A. Chapman, M. Yamauchi, C. Behrens, G. Raso, L. M. S. Soto, E. R. P. Cuentes, I. I. Wistuba, J. M. Kurie and D. L. Gibbons, *Nat Commun*, 2020, **11**, 4520.
196 H. Egan, O. Treacy, K. Lynch, N. A. Leonard, G. O'Malley, E. Reidy, A. O'Neill, S. M. Corry, K. D. Veirman, K. Vanderkerken, L. J. Egan, T. Ritter, A. M. Hogan, K. Redmond, L. Peng, J. Che, W. Gatlin, P. Jayaraman, M. Sheehan, A. Canney, S. O. Hynes, E. M. Kerr, P. D. Dunne, M. E. O'Dwyer and A. E. Ryan, *Cell Reports*, DOI:10.1016/j.celrep.2023.112475.
197 J. Cao, S. Pickup, C. Clendenin, B. Blouw, H. Choi, D. Kang, M. Rosen, P. J. O'Dwyer and R. Zhou, *Clin Cancer Res*, 2019, **25**, 2314–2322.
198 J. Xiao, H. Rahbar, D. S. Hippe, M. H. Rendi, E. U. Parker, N. Shekar, M. Hirano, K. J. Cheung and S. C. Partridge, *npj Breast Cancer*, 2021, **7**, 42.
199 X. Yin, P. Liu, C. Zhang, C. Pan, Y. Lu, Z. Wang, B. Luo, B. Du, A. Yang, Q. Wu, C. Gu and Y. Shi, *Journal of Magnetic Resonance Imaging*, DOI:10.1002/jmri.70060.
200 F. P. Fliedner, T. B. Engel, H. H. El-Ali, A. E. Hansen and A. Kjaer, *BMC Cancer*, 2020, **20**, 134.
201 M. Kwon, I. Youn, E. S. Ko and S.-H. Choi, *Sci Rep*, 2024, **14**, 7180.
202 L. Zhang, X. Long, M. Nijiati, T. Zhang, M. Li, Y. Deng, S. Kuang, Y. Xiao, J. Zhu, B. He, J. Chen, P. Rossman, K. J. Glaser, S. K. Venkatesh, R. L. Ehman and J. Wang, *Cancer Imaging*, 2021, **21**, 50.
203 PH Research, S.L., *A Pilot Trial of PEGPH20 (Pegylated Hyaluronidase) in Combination With Avelumab (Anti-PD-L1 MSB0010718C) in Chemotherapy Resistant Pancreatic Cancer*, clinicaltrials.gov, 2019.
204 Halozyme Therapeutics, *A Phase 1b/2 Multicenter, International, Randomized, Double Blind, Placebo-Controlled, Study of Gemcitabine Combined With PEGPH20 Compared to Gemcitabine Combined With Placebo in Patients With Stage IV Previously Untreated Pancreatic Cancer*, clinicaltrials.gov, 2018.
205 Pancreatic Cancer Research Team, *Phase II Study of PEGPH20 and Pembrolizumab (MK-3475) for Patients With Previously Treated Hyaluronan High (HA-High) Metastatic Pancreatic Ductal Adenocarcinoma*, clinicaltrials.gov, 2019.
206 Fox Chase Cancer Center, *Window of Opportunity for Neoadjuvant Stroma Modification in Pancreatic Cancer*, clinicaltrials.gov, 2025.
207 J. Wo, *A Randomized Phase 2 Study of Losartan and Nivolumab in Combination With FOLFIRINOX and SBRT in Localized Pancreatic Cancer*, clinicaltrials.gov, 2025.
208 C. D. Weekes, *A Phase II Study of FOLFIRINOX Combined With the Glycogen Synthase Kinase-3 Beta (GSK-3 β) Inhibitor 9-ING-41 and the Transforming Growth Factor-β (TGF-β) Inhibitor Losartan in Patients With Untreated Metastatic Pancreatic Cancer*, clinicaltrials.gov, 2025.
209 Providence Health & Services, *Phase II Study of TGFβ Type I Receptor Inhibitor LY2157299 With Neoadjuvant Chemoradiation in Patients With Locally Advanced Rectal Adenocarcinoma*, clinicaltrials.gov, 2025.
210 Eli Lilly and Company, *A Phase 1b/2 Study With Gemcitabine and LY2157299 for Patients With Metastatic Cancer (Phase 1b) and Advanced or Metastatic Unresectable Pancreatic Cancer (Phase 2)*, clinicaltrials.gov, 2018.
211 National Cancer Institute (NCI), *Cancer Stem Cells and Inhibition of Hedgehog Pathway Signaling in Advanced Pancreas Cancer: A Pilot Study of GDC-0449 in Combination With Gemcitabine*, clinicaltrials.gov, 2017.
212 University of Michigan Rogel Cancer Center, *VISmodegib for ORbital and Periocular Basal Cell Carcinoma (VISORB)*, clinicaltrials.gov, 2021.
213 FibroGen, *A Randomized, Open Label, Phase 1/2 Trial of Gemcitabine Plus Nab-paclitaxel With or Without FG-3019 as Neoadjuvant Chemotherapy in Locally Advanced, Unresectable Pancreatic Cancer*, clinicaltrials.gov, 2023.
214 China Medical University Hospital, *Treatment With Nivolumab and All-trans Retinoic Acid for Patients With Refractory Pancreatic Cancer*, clinicaltrials.gov, 2024.
215 University of Colorado, Denver, *Ipilimumab and All-Trans Retinoic Acid Combination Treatment of Advanced Melanoma*, clinicaltrials.gov, 2023.
216 Gilead Sciences, *A Phase 2 Randomized, Double-Blinded, Placebo-Controlled Study to Evaluate the Efficacy and Safety of GS-6624 Combined With Gemcitabine as First Line Treatment for Metastatic Pancreatic Adenocarcinoma*, clinicaltrials.gov, 2015.

217 N. Badri, *A Phase 1b/2 Trial of PXS-5505 Combined With First Line Atezolizumab Plus Bevacizumab For Treating Patients With Unresectable Hepatocellular Carcinoma*, clinicaltrials.gov, 2023.
218 AbbVie (prior sponsor, Abbott), *Phase 2 Open-Label Study of Volociximab (M200) in Combination With Gemcitabine in Patients With Metastatic Pancreatic Cancer Not Previously Treated With Chemotherapy*, clinicaltrials.gov, 2013.
219 Ikena Oncology, *A Phase 1, First-in-Human Study of IK-930, an Oral TEAD Inhibitor Targeting the Hippo Pathway in Subjects with Advanced Solid Tumors*, clinicaltrials.gov, 2024.
220 L. Zheng, *A Randomized Phase II Study of Pembrolizumab With or Without Defactinib, a Focal Adhesion Kinase Inhibitor Following Chemotherapy as a Neoadjuvant and Adjuvant Treatment for Resectable Pancreatic Ductal Adenocarcinoma (PDAC)*, clinicaltrials.gov, 2025.
221 T. Lookman, P. V. Balachandran, D. Xue and R. Yuan, *npj Comput Mater*, 2019, **5**, 21.
222 Y. Sverchkov and M. Craven, *PLoS Comput Biol*, 2017, **13**, e1005466.
223 A. G. Kusne, H. Yu, C. Wu, H. Zhang, J. Hattrick-Simpers, B. DeCost, S. Sarker, C. Oses, C. Toher, S. Curtarolo, A. V. Davydov, R. Agarwal, L. A. Bendersky, M. Li, A. Mehta and I. Takeuchi, *Nat Commun*, 2020, **11**, 5966.
224 B. Shahriari, K. Swersky, Z. Wang, R. P. Adams and N. De Freitas, *Proc. IEEE*, 2016, **104**, 148–175.
225 H. Yang, S. Hyeon Hong, R. ZhG and Y. Wang, *RSC Advances*, 2020, **10**, 13799–13814.
226 N. J. Treloar, N. Braniff, B. Ingalls and C. P. Barnes, *PLoS Comput Biol*, 2022, **18**, e1010695.